

TIDAL CHANNEL IDENTIFICATION FROM REMOTELY SENSED DATA USING SPECTRAL AND SHAPE CHARACTERISTICS

Bharat Lohani^{a,*}, B. Sreenivas^a

^aDepartment of Civil Engineering, IIT Kanpur, Kanpur 208016 (India)- blohani@iitk.ac.in

Commission IV WG-IV/10

KEY WORDS: Tidal channel, Image processing, Segmentation, Shape indices, Algorithm

ABSTRACT:

Mapping of tidal channels is significant and fundamental in intertidal hydrodynamic studies. This paper is an attempt to develop a new approach for tidal channel identification from remotely sensed data, by accounting for the spectral and shape properties of channels. The method begins with segmentation of the image ensuring similarity of neighbouring pixels in each segment. A few training pixels selected in the channels locate the training channel segments. The image is classified in non-channel and channel segments based on the statistical similarity, which is established here by T^2 statistic, of unknown segments to known channel segments. It is obvious at this stage, owing to the spectral complexity of tidal regions, that several non-channel areas are also classified as channels. The curvilinear shape of channels, which is established using shape indices, is used to eliminate the falsely classified non-channel areas. The paper presents the methodology and some initial results obtained. It also outlines the scope for further research.

1. INTRODUCTION

Tidal channel networks are significant and fundamental for the study of tidal hydrodynamics (Fagherazzi et al. 1999, Pethick 1992, Rodriguez-Iturbe and Rinaldo 1997). Mapping these channels through field surveying is a time-consuming and error-prone process. The remotely sensed data offer considerable potential for channel mapping. The channels may be manually traced from remotely sensed data as is conventionally done. However, this approach is fraught with several problems (Lohani et al., 2006). In view of this, there have been several attempts to identify channels from remotely sensed data through computer-based methods (Fagherazzi et al. 1999; Lohani and Mason, 2001; Mason et al., submitted). Use of DEM based methods has not been found suitable for tidal channels (Lohani, 1999). However, the image processing based methods have shown considerable potential for both geometric (LiDAR) and spectral (multispectral) data.

The approach suggested by Lohani et al. (2006) for identification of channel networks from multispectral images is based on the feature-constrained classification. In this method the edges in the image are detected and localised. The anti-parallel edge pairs of channels and also non-channel areas are associated using a distance-with-destination transform. The centrelines of channels and non-channel areas are also located with the help of this transform. Training data are collected from a statistically similar and small neighbourhood of a selected seed pixel. A multiple of these neighbourhoods pooled together results in a set of pixels as training samples. The unknown pixels of image are classified as channel or non-channel based on a rule which checks their Mahalanobis distance from training data. Beginning from the seed pixels selected by user the

centrelines of channels are extended if these are continuous and also classified everywhere as channels. This results in as many channel segments as there are seed pixels. The final step extrapolates these segments at their endpoints and joins these with other segments, which are classified as channels but were not connected to the seed pixel. The results obtained by this method are acceptable. However, the method fails to distinguish between error blobs (non-channel areas which are spectrally similar to channels and also connected to channels by centrelines) and curvilinear channels. Further, the method classifies pixels as channels and non-channels without accounting for their neighbourhood.

This paper describes a new approach, which is an improvement on the method described above. This method produces equivalent or better results while minimising the limitations of the above method. Furthermore, the proposed method conforms better to the inherent spectral and spatial characteristics of tidal channels, thereby promising a more generic solution.

2. DATA USED

The multispectral data used in this paper is the TopoSys linescanner image of the lagoon of Venice in Italy (**Figure 1 (a)**). The image was captured at low water on October 2002. The image consists of near infrared, red, green, and blue bands and has 1000 by 1000 size. The other data used is from Morecambe Bay in UK (**Figure 1(b)**). The Morecambe Bay image (400*600) is comprised of red, green and blue bands and was obtained on June 2000. The spatial resolution of both images (Morecambe Bay photo scale 1:10000, Venice

* Corresponding author

Linescanner pixel size 0.5m) is sufficient to map the majority of the channels.

3. CHANNEL IDENTIFICATION

The various image-processing steps employed for channel identification are discussed in the following paragraphs.

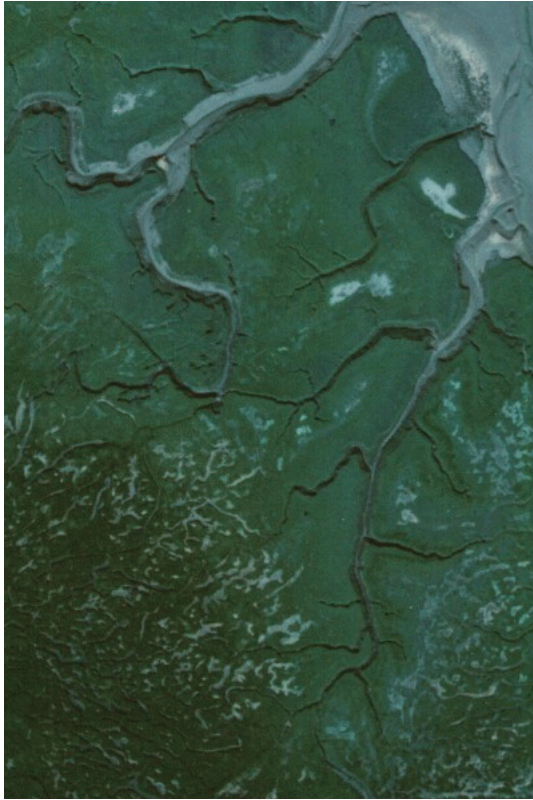
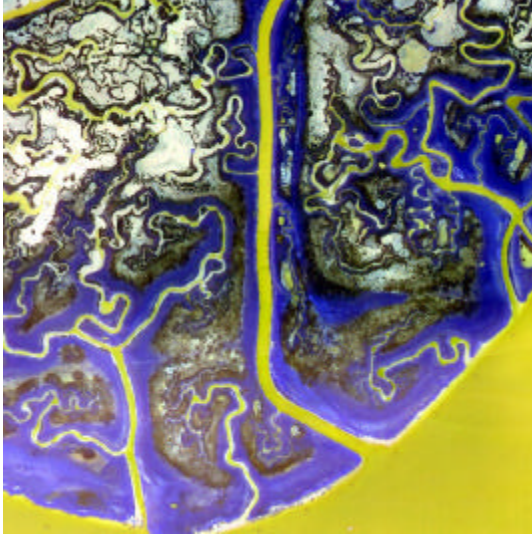


Figure 1: (a) Linescanner image of part of Venice Lagoon; (b) Aerial photograph of part of Morecambe Bay in U.K.

3.1 Determination of threshold

Selection of an appropriate threshold is a crucial step in a region-based segmentation. An arbitrary threshold may yield a useless segmentation. In present work the Otsu method (Otsu, 1979) has been employed to find the threshold value. An optimal threshold is selected by the discriminant criterion to maximize the separation of the resultant classes. The formulation of the objective function is as follows:

$$S_B^2(k) = \frac{[\mathbf{m}_T \mathbf{w}(k) - \mathbf{m}(k)]^2}{\mathbf{w}(k)[1 - \mathbf{w}(k)]} \quad (1)$$

where,

$$\mathbf{m}_T = \mathbf{m}(L) = \sum_{i=1}^L ip_i$$

i.e., the global mean in the window of interest which may be of any size. L is dynamic range of image. Here p_i is the probability of occurrence of grey level i in the window of interest.

Further,

$$\mathbf{w}(k) = \sum_{i=1}^k p_i \quad \text{and} \quad \mathbf{m}(k) = \sum_{i=1}^k ip_i$$

are the cumulative probability and grey level mean up to the grey value of k . The optimal threshold k^* is determined by:

$$S_B^2(k^*) = \max_{1 \leq k \leq L} S_B^2(k)$$

To implement this, a differenced image is derived from original image using the operator:

$$d(i, j) = \text{Max} |x(i, j) - x(i+k, j+l)| \quad (2)$$

for $-1 \leq k \leq 1$ and $-1 \leq l \leq 1$

Where $x(i, j)$ and $d(i, j)$ are the grey level and differential value respectively at pixel (i, j) and k and l are integers.

An odd sized window (5 by 5 in the present case) is run over this differenced image to determine the threshold value for each window position using the objective function discussed above. The threshold value with highest frequency of occurrence for all window positions is selected as the global threshold value. Using this operation the threshold value has been found for each spectral band of the multi-spectral data set. Threshold values obtained for Venice image are 27, 28 and 28 for green, red and infrared bands, respectively. For Morecambe Bay photograph the threshold values are 14, 14 and 13 for red, green and blue bands, respectively.

3.2 Region growing

After finding the threshold value for each band, region growing is started from the very first pixel in the image. At this stage, a region is initiated and a label is assigned to it. All the neighbouring pixels of this pixel are assessed for their inclusion

in the current region. A pixel will be included in a region if the difference between this pixel and the current region mean is less than the threshold value in all the bands. For region growing eight-connected neighbours of a pixel are considered for inclusion in the segment. A region will stop growing when no new pixels are added to it and a new region will be initiated from the next pixel which is not included in any region. This process continues till every pixel in the image gets included in one of the regions. The output of this process is a segment image with a label number assigned to each segment.

3.3 Segment-based classification

Having obtained the segment image, the next step is to classify each segment as channel or non-channel segment. As a first step the user selects a few pixels in the channel area on the FCC (False Colour Composite) of the image (50 for the present cases). The segments in which these seed pixels lie become the training segments. The spectral property of channels in an image varies with space and time, thus resulting in training segment, with different spectral properties. The classification scheme adopted aims at classifying the entire unknown segment instead of its individual pixels, based on its statistical nearness to the training segments. The unknown segments which are found statistically similar to any of the training segments are classified as channel segments, while the rest of the segments are classified as non-channel.

In the present work a multivariate analysis approach is used to classify the images. In this approach an inference will be made about $\mathbf{m}_1 - \mathbf{m}_2$, where μ_1 and μ_2 are the mean vectors of population 1 and population 2, respectively. A squared statistical distance T^2 is computed for testing the equality of vector means (i.e. testing the hypothesis $H_0 : \mathbf{m}_1 - \mathbf{m}_2 = 0$) from two multivariate populations. This statistic is computed using the following expression (Jhonson and Wichen, 1982).

$$T^2 = [\bar{X}_1 - \bar{X}_2]^T \left[\frac{1}{N_1} S_1 + \frac{1}{N_2} S_2 \right]^{-1} [\bar{X}_1 - \bar{X}_2] \quad (3)$$

Where:

- \bar{X}_1, \bar{X}_2 are mean vectors of known and unknown segments, respectively
- S_1, S_2 are variance-covariance matrices of known and unknown segments, respectively
- N_1, N_2 are the number of pixels of known and unknown segments, respectively.

Complexities may arise due to unequal variance-covariance matrices, but are avoided because of large sample sizes (i.e. N_1, N_2). This squared distance has an approximate \mathbf{c}^2 -distribution. After computing the statistic, it is tested against a critical value which is derived from $\mathbf{c}_n^2(\mathbf{a})$ -distribution, where \mathbf{a} is the significance level and n is the degrees of freedom

(95% and 3, respectively, here.) If the statistic T^2 comes greater than the critical value the hypothesis will be rejected, i.e., the vector mean of unknown segment differs from that of known segment. In this way all candidate regions, which qualify to be classified as channel area, are identified. The classified images are shown in Figure 2.

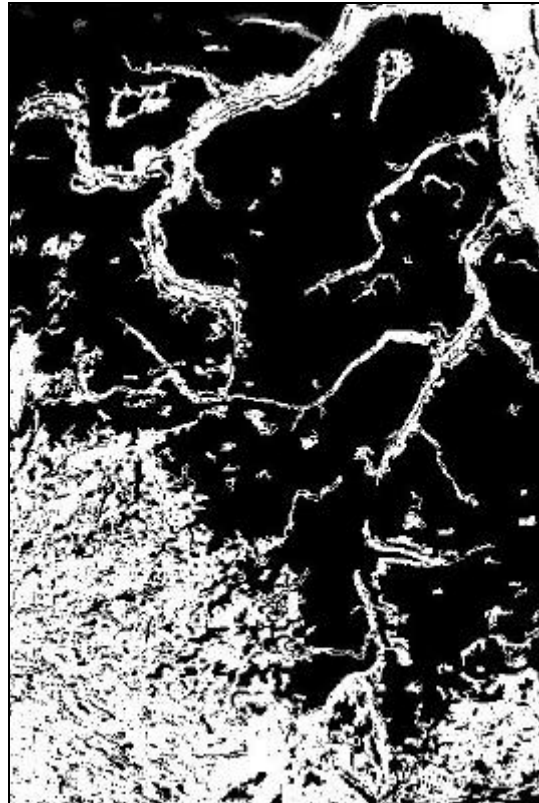
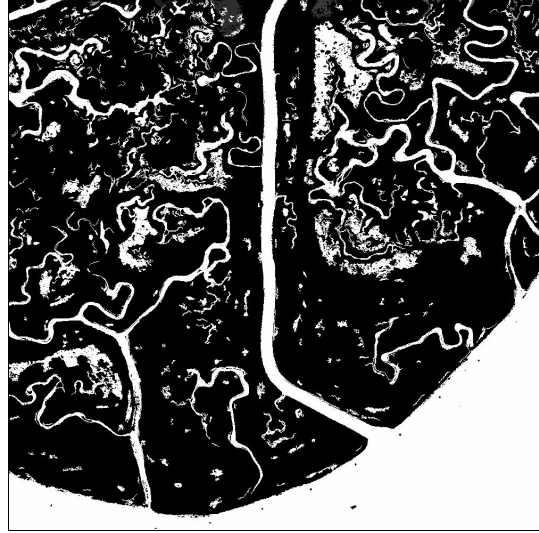


Figure 2: Result of segment-based classification. Non-channel areas also appear along with channels.

3.4 Shape analysis

Not all segments classified as channel in the above step are channel on the ground. This is because the spectral property of some non-channel areas is similar to that of channels. These segments are part of intertidal mud flats or depressions in mud flats that are moist or filled with water or saltmarsh vegetation regions etc. In manual interpretation of remotely sensed data these segments are not classified as channels due to their non-connectivity to the major channel network and, more importantly, due to their unlike-a-channel shape. The channels are characterized by their curvilinear shape and connectivity to a network. While the latter can be ensured by channel joining mechanism (Lohani et al., 2006) the former is employed here to distinguish channel from non-channel areas in the classified images.

To realise the above, shape analysis is performed on all the candidate regions in the classified image. Two shape parameters, namely Extent and Elongation are employed jointly to detect and reject the blob shaped non-channel segments. They are calculated as:

$$\text{Extent} = \frac{\text{net area of the region}}{\text{area of bounding rectangle of the region}} \quad (4)$$

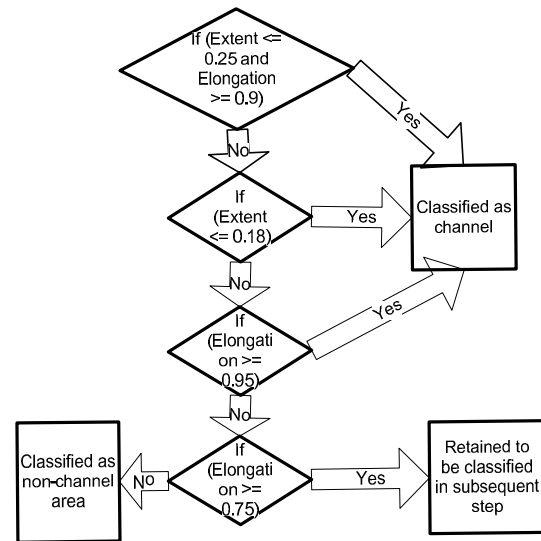
$$\text{Elongation} = \frac{\text{major axis}}{\text{minor axis} + \text{major axis}}$$

Major axis is the direction in which the spread of segment is more. Perpendicular to the major axis is the minor axis. The approach to extract shape features is based on the concept of eigenvalues (Costa and Cesar, 2001). The lengths of the major and minor axis are defined as the associated eigenvalues. The eigenvalues are computed using the boundary pixels of a region. The shape measure Extent will be smaller for thin and elongated regions, i.e. channels. However, this is not true for thin and elongated regions that are nearly vertical or horizontal. In these situations to identify these segments as channels the second shape measure, i.e., Elongation is employed. The conditions shown in the flowchart (Figure 3) are imposed on candidate regions in order to classify them as channel or non-channel. There are three classes of segments at the end of the first step (Figure 3(a)), i.e., channels, non-channels and those which have potential to be classified as channels but need further confirmation, which is realised in the subsequent process (Figure 3(b)). In this step, the suspect segment is classified as channel provided it is a neighbour of an already classified channel, has the desired shape properties and is spectrally similar to its said channel neighbour.

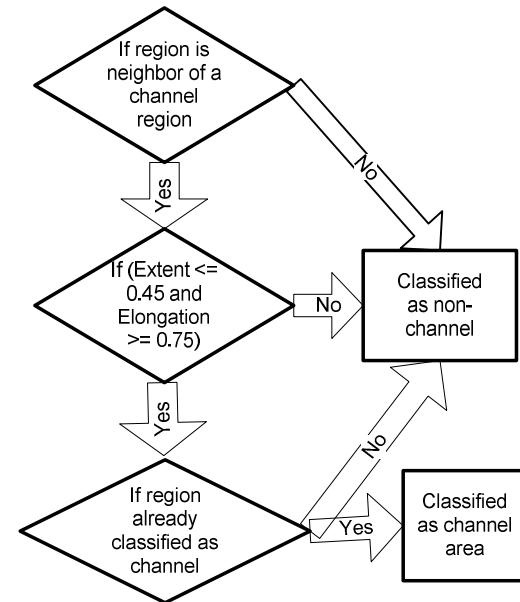
The strategy adopted works well in identifying isolated non-channel segments. However, it fails in case of segments that consist of a non-channel blob and a channel joined together, as shown in Figure 4. These blobs were cleaned by scanning all segments in horizontal and vertical to determine their width at the level of scan (i.e. at each scan line and column of image). This width was compared with the maxima width at the locations of seed pixels. Those parts of the segment where its width is larger than maxima channel width in both directions are deleted from segment. This operation serves to cut off the blobs from the channels.

The channel images with finally identified channels are shown in Figure 5. It can be noticed in this image that most of the blob shaped features of Figure 2 have been eliminated.

In order to assess the accuracy of identification validation data are prepared by manually tracing the channels from images shown in Figure 1. The comparison (pixel by pixel) shows that for Venice data 52% of channel area is correctly identified while the errors of omission and commission are 48% and 14%, respectively. For Morecambe Bay aerial photograph the correctly identified pixels are 51% while the omitted and committed areas are 49% and 30%, respectively. The overall performance of this method is similar to the method proposed in Lohani et al. (2006). Moreover, with the attempt to join channels, as done in Lohani et al. (2006), the performance should improve.



(a)



(b)

Figure 3: Flow diagram for channel identification using Extent and Elongation jointly. The retained segments in (a) are fed in (b).

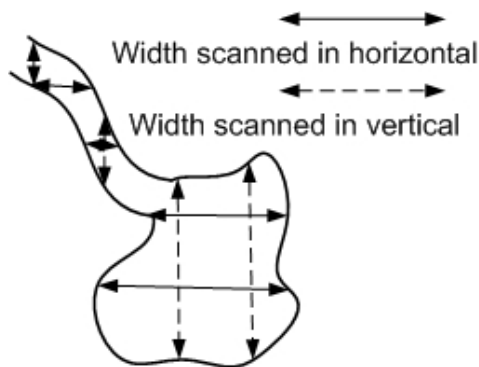


Figure 4: Elimination of non-channel segment part using scanned widths in horizontal and vertical.

4. CONCLUSION

The method proposed is closure in emulating manual interpretation as it accounts for both shape and spectral properties of channels. This is a more generic approach to solve the problem of channel identification. In the presently adopted segmentation method it was noted that some of the resulting segments were not pure, with some being even bi-modal. A better method of segmentation, which should work on adaptive instead of global threshold, should improve segmentation. Further attempts are being made to employ better segment classification procedures, e.g., classification of a segment based on the joint likelihood, of all pixels in the segment of belonging to training segment (determined using Maximum Likelihood algorithm).

5. ACKNOWLEDGEMENT

Thanks are due to Dr. David C Mason of the University of Reading for discussions and Morecambe Bay data and to TopoSys Ltd. for the provision of linescanner data of the Venice Lagoon. This work followed as a sequence of a previous work, which was funded under the Italian Government's CORILA project and the EU FP5 TIDE (Tidal Inlet Dynamics and Environment) project (EVK3-CT-2001-00064).

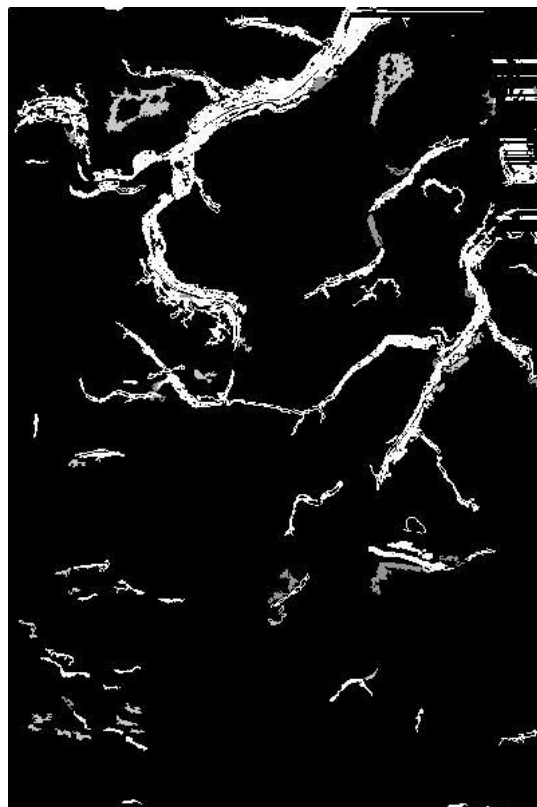
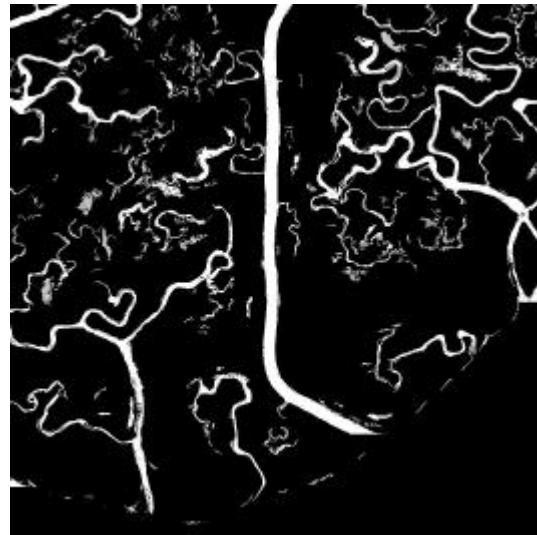


Figure 5: Final channel images for Venice lines scanner data and Morecambe Bay photograph.

6. REFERENCES

Costa, L d. F., and Cesar, R. M. Jr., 2001, *Shape Analysis and Classification: Theory and Practice*, 1st edn (New York: CRC Press).

Fagherazzi, S., Bortoluzzi, A., Dietrich, W. E., Rodriguez-Iturbe, I., Adami, A., Lanzoni, S., Marani, M., and Rinaldo, A., 1999, Tidal networks I: automatic network extraction and some scaling features from DTMs. *Water Resources Research*, 35(12),3891-3904.

Jhonson, R. A. and Wichern, D. W., 1982, *Applied Multivariate Statistical Analysis*, 1st edn (New Jersey: Prentice Hall).

Lohani, B., 1999. Application of Airborne Remote Sensing to the study of Intertidal zone, Ph. D. thesis, The University of Reading, Reading, UK.

Lohani, B., and Mason, D. C., 2001, Application of airborne scanning laser altimetry to the study of tidal channel geomorphology. *ISPRS Jr. Photogrammetry and Remote Sensing*, 56, 100-120.

Lohani, B., Mason, D. C., Scott, T. R., and Sreenivas, B., 2006, Identification of tidal channel networks from aerial photographs alone and fused with airborne laser altimetry, *International Journal of Remote Sensing*, 27(1), 5-25

Mason, D. C., Scott, T.R. and Wang, H-J., Extraction of tidal channel networks from airborne scanning laser altimetry, *ISPRS Jr. Photogrammetry and Remote Sensing (submitted)*.

Otsu, N., 1979, A threshold selection method from grey-level histograms, *IEEE Transactions on systems, Man, and Cybernetics*, SMC-9, 62-66.

Pethick, J. S., 1992, Saltmarsh geomorphology. In *Saltmarshes, Morphology, Conservation and Engineering Significance*, edited by J. R. L. Allen and K. Pye (Cambridge: Cambridge University Press), pp. 41 - 62.

Rodriguez-Iturbe, I., and Rinaldo, A., 1997, Fractal River Basins: *Chance and Self-Organisation*, 1st edn (New York: Cambridge University Press).